

Bias-induced reconstruction of hybrid interface states in magnetic molecular junctions

Ling-Mei Zhang(张令梅)†, Yuan-Yuan Miao(苗圆圆)†, Zhi-Peng Cao(曹智鹏), Shuai Qiu(邱帅), Guang-Ping Zhang(张广平), Jun-Feng Ren(任俊峰), Chuan-Kui Wang(王传奎), and Gui-Chao Hu(胡贵超)‡

Citation: Chin. Phys. B, 2022, 31 (**5**): 057303. DOI: 10.1088/1674-1056/ac3caf
Journal homepage: http://cpb.iphy.ac.cn; http://iopscience.iop.org/cpb

What follows is a list of articles you may be interested in

Preparation of PSFO and LPSFO nanofibers by electrospinning and their electronic transport and magnetic properties

Ying Su(苏影), Dong-Yang Zhu(朱东阳), Ting-Ting Zhang(张亭亭), Yu-Rui Zhang(张玉瑞), Wen-Peng Han(韩文鹏), Jun Zhang(张俊), Seeram Ramakrishna, and Yun-Ze Long(龙云泽)

Chin. Phys. B, 2022, 31 (**5**): 057305. DOI: 10.1088/1674-1056/ac3baa

Bias-induced reconstruction of hybrid interface states in magnetic molecular junctions

Ling-Mei Zhang(张令梅)†, Yuan-Yuan Miao(苗圆圆)†, Zhi-Peng Cao(曹智鹏), Shuai Qiu(邱帅), Guang-Ping Zhang(张广平), Jun-Feng Ren(任俊峰), Chuan-Kui Wang(王传奎), and Gui-Chao Hu(胡贵超)‡

Chin. Phys. B, 2022, 31 (**5**): 057303. DOI: 10.1088/1674-1056/ac3caf

Spin transport properties for B-doped zigzag silicene nanoribbons with different edge hydrogenations

Jing-Fen Zhao(赵敬芬), Hui Wang(王辉), Zai-Fa Yang(杨在发), Hui Gao(高慧), Hong-Xia Bu(步红霞), and Xiao-Juan Yuan(袁晓娟)

Chin. Phys. B, 2022, 31 (**1**): 017302. DOI: 10.1088/1674-1056/ac0795

Magneto-transport properties of thin flakes of Weyl semiconductor tellurium

Nan Zhang(张南), Bin Cheng(程斌), Hui Li(李惠), Lin Li(李林), and Chang-Gan Zeng(曾长淦)

Chin. Phys. B, 2021, 30 (**8**): 087304. DOI: 10.1088/1674-1056/ac0a5e

Three-dimensional Monte Carlo simulation of bulk fin field effect transistor

Wang Jun-Cheng, Du Gang, Wei Kang-Liang , Zhang Xing, Liu Xiao-Yan

Chin. Phys. B, 2012, 21 (**11**): 117308. DOI: 10.1088/1674-1056/21/11/117308

Bias-induced reconstruction of hybrid interface states in magnetic molecular junctions

Ling-Mei Zhang(张令梅)[†], Yuan-Yuan Miao(苗圆圆)[†], Zhi-Peng Cao(曹智鹏), Shuai Qiu(邱帅), Guang-Ping Zhang(张广平), Jun-Feng Ren(任俊峰), Chuan-Kui Wang(王传奎), and Gui-Chao Hu(胡贵超)[‡]

Shandong Provincial Key Laboratory of Medical Physics and Image Processing Technology, School of Physics and Electronics, Shandong Normal University, Jinan 250358, *China*

(Received 26 September 2021; revised manuscript received 22 November 2021; accepted manuscript online 24 November 2021)

Based on first-principles calculations, the bias-induced evolutions of hybrid interface states in π-conjugated tricene and in insulating octane magnetic molecular junctions are investigated. Obvious bias-induced splitting and energy shift of the spin-resolved hybrid interface states are observed in the two junctions. The recombination of the shifted hybrid interface states from different interfaces makes the spin polarization around the Fermi energy strongly bias-dependent. The transport calculations demonstrate that in the π-conjugated tricene junction, the bias-dependent hybrid interface states work efficiently for large current, current spin polarization, and distinct tunneling magnetoresistance. But in the insulating octane junction, the spin-dependent transport via the hybrid interface states is inhibited, which is only slightly disturbed by the bias. This work reveals the phenomenon of bias-induced reconstruction of hybrid interface states in molecular spinterface devices, and the underlying role of conjugated molecular orbitals in the transport ability of hybrid interface states.

Keywords: molecular spinterface, hybrid interface states, bias effect

PACS: 73.63.–b, 75.47.–m, 85.75.–d **DOI:** 10.1088/1674-1056/ac3caf

1. Introduction

The application of organic molecules to spintronics has formed a new field, called organic spintronics,[1–10] and aroused widespread interest due to the pursuit of flexible and low-cost devices with advanced performances.[11–14]

Recently, another advantage of organic molecules in interface modification, *i.e.*, the generation of hybrid interface states (HISs) between ferromagnetic metals and organic molecules, has been widely noticed.[15–17] When an organic molecule is adsorbed onto the ferromagnetic surface, the orbital hybridization may occur at the interface, which may change the interfacial spin polarization (SP) significantly. The SP at the ferromagnetic/molecular interface can be further modulated by manipulating interface morphology or molecular structure, thus setting up a new field of molecular spinterface,[18,19] that is, a field in which the metal/organic interfaces are important and specially designed for spin applications.

Manipulation of HIS and interfacial SP have been investigated extensively in past years. For example, according to the first-principles calculations, Atodiresei *et al*. demonstrated that the p_z–d hybridization between C atoms and Fe atoms is the mechanism of the SP inversion at organic sites.[20] Subsequently, Djeghloul *et al*. experimentally confirmed the contribution of sp^3–d orbital hybridization to interfacial SP by using alkane molecules.[21] Some subsequent researches further confirmed the controllability of the interfacial SP. For example, it was found that the interface magnetic moment and spin polarization can be changed by replacing the H atoms in the benzene ring with Cl or F atoms.[22] Qiu *et al*. showed the modulation of HIS via molecular geometric torsion and anchoring groups in magnetic molecular junctions.[23,24]

In consideration of the controllable SP of HIS, exploring the role of HIS in spin-dependent transport and even designing functional molecular spin devices are of high interest and importance. The HISs usually exist in the molecular gap near the Fermi energy and belong to the metal induced gap states,[25,26] which are crucial in determining the transport properties of the device. For example, in LSMO/Alq_3/Co organic spin valve, the diversity of magnetoresistance is attributed to the distinct SP of the HIS.[27] It was also found that by controlling the SP of HIS via destructive quantum interference, the SP of the current can be modulated.[28] However, we noticed that in most of devices the functionality is usually assumed according to their SP property at a single interface. In a real molecular device, the junction is composed of two interfaces, with an external bias applied. The HIS and their SP will be adjusted by bias because of the localized characteristics of HIS. Up to now, the details of HIS evolution under bias have remained unclear. In this work, we address the following questions: (i) how do the HISs as well as their SP evolve with the bias voltage increasing? (ii) How does the transmission spectrum of the HIS change with the bias voltage increasing? (iii) What are the effects on the SP of current and magnetoresistance, caused by

[†]These authors contributed equally to this work.

[‡]Corresponding author. E-mail: hgc@sdnu.edu.cn

© 2022 Chinese Physical Society and IOP Publishing Ltd

the above changes?

In order to answer the above questions, two typical molecules, tricene and octane, are connected to two Ni electrodes via S atoms. The former molecule owns conjugated π orbitals while the latter one is insulating from the sp^3 hybridized orbitals. The rest of this paper is organized as follows. In Section 2 theoretical models and calculation details are introduced. In section 3, the effects of bias on the SP and the spin-dependent transport properties of the HIS are exhibited and discussed. Finally, some conclusions are drawn in Section 4.

2. Theoretical models and calculation details

Here we consider two molecular junctions, *i.e.*, a conjugated tricene molecule and a non-conjugated octane molecule sandwiched between two nickel electrodes. The Ni (111) surface is determined by a triangle consisting of three nickel atoms out of the plane. These molecules attach to hollow positions on the three nickel atoms via S anchoring groups as shown schematically in Fig. 1, which is widely used in theoretical and experimental studies of molecular electronics.[29,30] The molecular junction is divided into three parts: the left and right semi-infinite electrode and the central scattering region. The semi-infinite Ni electrode is simulated by a $3\times4\times3$ element with a periodic boundary in x and y directions perpendicular to the transport direction. The central scattering region is composed of the molecule and six layers of Ni electrode on each side.

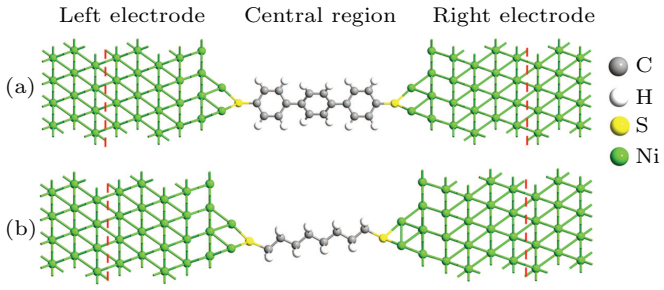


Fig. 1. Schematic diagram of (a) Ni/tricene/Ni and (b) Ni/octane/Ni magnetic junctions.

In Atomistix ToolKit (ATK) package,[31,32] the molecule is first optimized with a maximum residual force of 0.04 eV/Å. Then the molecule is connected to two Ni electrodes by the S atom, and the central region of the junction is optimized again. For Ni atoms the single zeta-polarized (SZP) basis set is adopted, and for other atoms the double zeta-polarized (DZP) basis set is used. Spin-dependent generalized gradient approximation (SGGA) Perdew–Burke–Ernzerhof (PBE)[33] is selected as the exchange and correlation functional, and Troullier–Martins-type norm-conserving pseudopotential[34] is used. In the self-consistent loop, tolerance convergence is selected as 1.0×10^{-4} Hartree (1 Hartree = 4.3597×10^{-18} J) and a density mesh cut-off of 300 Rydberg (1 Ry = 13.6056923(12) eV) is used. In the x, y, and z directions, a $3\times3\times100$ k-point in Brillouin-zone (BZ) is adopted.

The spin-resolved current at a bias voltage V is calculated by using the Landauer–Büttiker formula[35]

$$I_\sigma(V)=\frac{e}{h}\int_{\mu_L}^{\mu_R}T_\sigma(E,V)\left[f_L(E-\mu_L)-f_R(E-\mu_R)\right]\mathrm{d}E, \quad (1)$$

where $\sigma=\uparrow/\downarrow$ is the spin index of the electron, e and h are the electron charge and Planck's constant, $f_{L/R}\left(E-\mu_{L/R}\right)$ is the Fermi–Dirac distribution function of electron in the left/right electrode with the electrochemical potential $\mu_{L/R}$, $T_\sigma(E,V)$ is the transmission function under bias voltage V at energy E of spin σ, and expressed as[36]

$$T_\sigma(E,V)=\mathrm{tr}\left[\Gamma_\sigma^L(E,V)G_\sigma(E,V)\Gamma_\sigma^R(E,V)G_\sigma^+(E,V)\right]. \quad (2)$$

Here, $G_\sigma(E,V)/G_\sigma^+(E,V)$ is the spin-dependent retarded/advanced Green's function in the central region at bias voltage V. The $G_\sigma(E,V)$ is expressed as

$$G_\sigma(E,V)=\left[(E+\mathrm{i}\delta_+)S-H_M^\sigma-\Sigma_L(E,V)-\Sigma_R(E,V)\right]^{-1}. \quad (3)$$

Here, δ_+ is an infinitely small quantity, S is an overlap matrix, H_M^σ is the Hamiltonian of the central region, $\Sigma_{L/R}(E,V)$ is the self-energy due to the coupling with the left/right electrode, and $\Gamma_\sigma^{L/R}(E,V)$ is the broadening function of the left /right electrode. The total current through the molecular junction under the bias can be obtained by summing the currents with different spins.

3. Results and discussion

The magnetic junction is constructed by connecting each molecule with two Ni electrodes through the S atoms. The spin configurations of the two Ni electrodes can be parallel (P) or antiparallel (AP).[37] Before investigating the bias-induced evolution of the HIS, we first analyze the properties of the HIS for the two different molecules under zero bias voltage. The projected density of states (PDOS) of the two molecules in P configuration is shown in Fig. 2. The eigenvalues of the molecular projected self-consistent Hamiltonian (MPSH)[38] are also marked. Apparently, spin-polarized HISs appear in the energy gap for both molecules without corresponding to any MPSH eigenvalue. For the aromatic molecule tricene with conjugated π orbitals, we notice that three obvious HIS peaks emerge near the Fermi energy. Two spin-down peaks are located at about 0.14 eV above the Fermi energy and -1.05 eV below the Fermi energy, respectively. A spin-up peak is observed at about -0.9 eV. The HISs are different from the Ni/benzene-dithiolate/Ni system although the anchoring atoms are identical.[39] By further projecting the DOS onto

the tricene and the left/right S atom, it can be found that each S atom and the tricene contribute almost equally to the HIS below the Fermi energy, while a larger portion from the tricene is found for the HIS above the Fermi energy. For the octane molecule without π orbitals, enormous HISs appear below the Fermi energy except a spin-down HIS peak at 0.23 eV above the Fermi energy. Further projection onto the molecular components indicates that the HIS near the Fermi energy is produced mainly by the S atom rather than the octane molecule. From the above results, one can conclude that molecular orbitals also participate in the interfacial hybridization other than the terminal anchoring atoms, especially for the π orbitals.

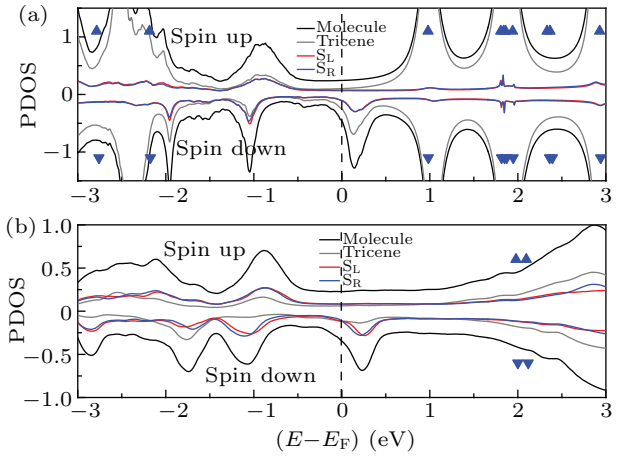


Fig. 2. PDOS of (a) tricene and (b) octane spin valves in P configuration. The PDOS is further projected onto molecule without S atoms or left S (S_L) or right S (S_R), respectively. The inserted triangles are MPSH eigenvalues of the whole molecule. The bias is zero.

The localization of the HIS in the two molecular junctions is further explored. In Fig. 3, we choose three HIS peaks the nearest to the Fermi energy and plot the local density of states (LDOS) of the HISs on each atom. It can be clearly found that for the tricene molecular junction, the HISs spread over the interfacial Ni atoms, S atoms and the nearest benzene rings, which confirms the participation of the molecular orbitals in the formation of HIS. However, for the octane molecular junction, we can barely see the electron distribution on the octane molecule, and the HISs are dominated by the interfacial Ni and S atoms.

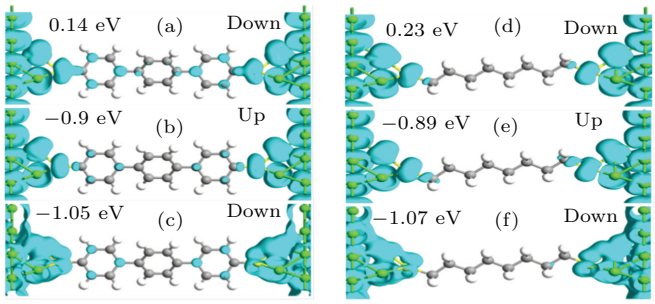


Fig. 3. LDOSs for the HIS near the Fermi energy. Isovalues are fixed at 0.02 for all plots.

The SP of the molecular PDOS is also calculated as shown in Fig. 4. Here the SP is defined as $\mathrm{SP}(E) = \left[\mathrm{PDOS}_{\uparrow}(E) - \mathrm{PDOS}_{\downarrow}(E)\right] / \left[\mathrm{PDOS}_{\uparrow}(E) + \mathrm{PDOS}_{\downarrow}(E)\right]$. For both molecules, the SP shows a similar trend as a broad spin-up peak below the Fermi energy, and a spin-down peak spans the Fermi energy. The maximum SP value of the tricene molecule is larger than that of the octane molecule. At the Fermi energy, the SP is about -33% for thetricene, and -21% for octane molecules.

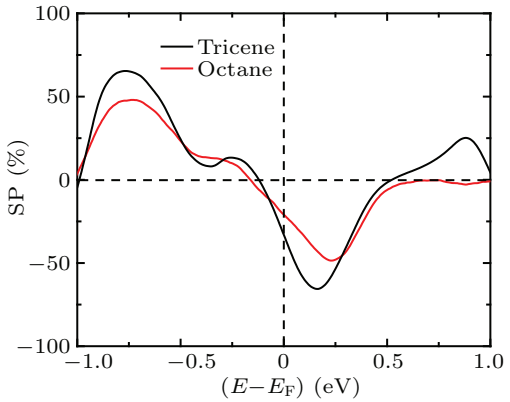


Fig. 4. Curves of spin polarization *versus* energy of molecular PDOS under zero bias in P configuration.

Now we focus on the evolution of the HIS in the presence of bias voltage. The bias-dependent PDOS of the two molecules in P configuration is shown in Fig. 5. For the tricene molecule, two kinds of different responses of the PDOS to the bias are clearly observed. The PDOS of molecular orbitals with corresponding MPSH eigenvalues are only slightly disturbed by bias, while the HISs near the Fermi energy are split obviously. Specifically, we take the spin-down HIS peak the nearest to the Fermi energy for example. At 0.4 V, such a peak is divided into two parts which move in opposite directions. The left peak toward the Fermi energy is contributed from the left S atom and the tricene molecule. The right one toward the upper molecular orbitals comes from the right S atom and the tricene molecule. This is because the positive bias lowers the chemical potential of the left electrode and lifts that of the right electrode. Thus, the interfacial hybridization at the two interfaces is not degenerate again and neither are their HISs. The obvious shift of the HIS in energy, rather than the molecular orbitals, origins from the high localization of the HIS, which follows the variation of the chemical potential of the neighbor electrode. With the increase of bias, the separation of the two split HIS is enhanced. Such a splitting and an energy shift are observed for all the HIS peaks near the Fermi energy. For the octane molecule without conjugated orbitals, a similar evolution occurs for the HIS except the absence of the molecular orbitals in this process. We also notice a small shift for MPSH eigenvalues. For the tricene molecule, the highest occupied molecular orbital (HOMO) gradually approaches to the Fermi energy, while the lowest unoccupied molecular orbital (LUMO) is hardly disturbed. For the octane molecule, an obvious red shift to the LUMO is observed.

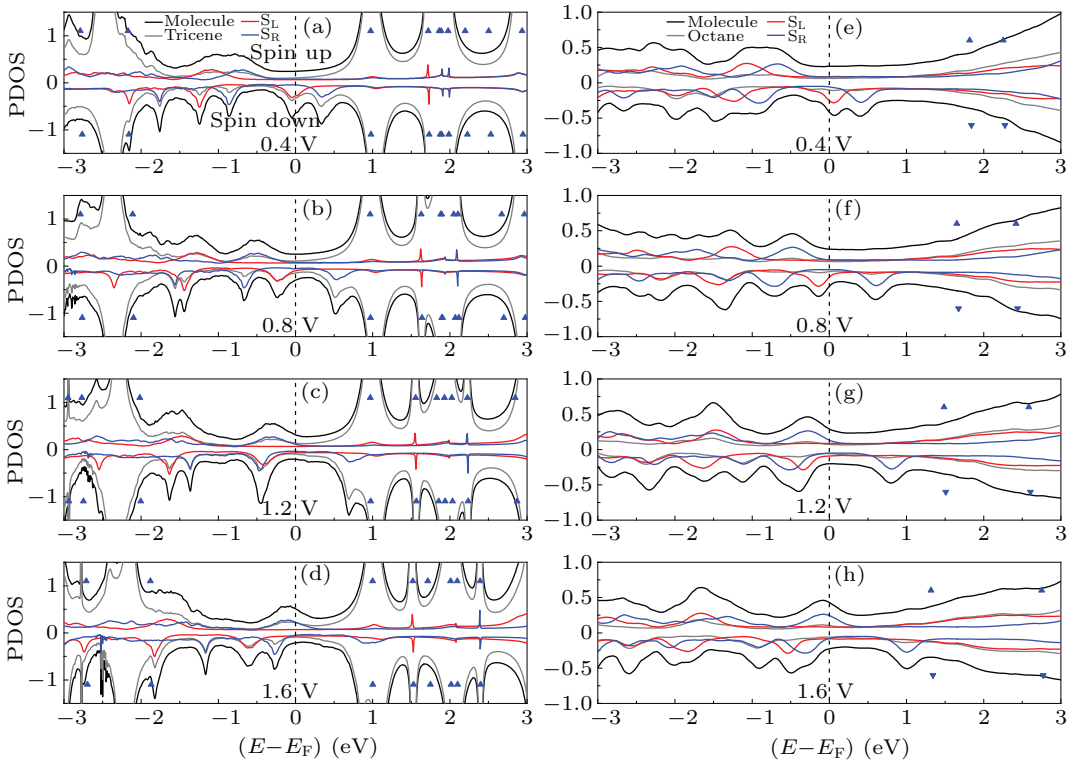


Fig. 5. Bias-dependent PDOSs of [(a)–(d)] tricene and [(e)–(h)] octane molecules. The PDOS is further projected onto the molecule without S atoms or left S or right S respectively. The inserted triangles are the MPSH eigenvalues of the molecule.

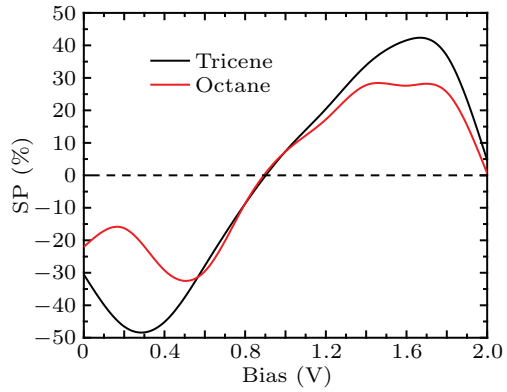


Fig. 6. Curves of bias-dependent spin polarization of molecular PDOS at Fermi energy in P configuration.

An interesting concomitant phenomenon brought by the splitting and shift of the HIS is that the SP around the Fermi energy is modulated by bias. For example, at 0.4 V, as shown in Fig. 5(a) the SP at the Fermi energy is negative due to the presence of the spin-down HIS. As the bias voltage is increased to 0.8 V and 1.2 V, the spin-down HIS is gradually shifted below the Fermi energy while a spin-up HIS peak is getting close to the Fermi energy. At 1.6 V, the PDOS at the Fermi energy is dominated by the spin-up HIS peak and the SP is reversed to positive value. In Fig. 6, the bias-dependent SP at the Fermi energy is plotted in the P configuration. A sign reversal of the SP from negative to positive is clearly observed at 0.9 V for the two molecular junctions. Below 0.9 V, the maximum value of the SP is about -48% (-33%) for the tricene (octane) molecule. After that, the maximum value of the SP achieves about 42% (28%) for the tricene (octane) molecule. Thus, in spite of the similar interfacial hybridization, the conjugated molecule corresponds to a little larger SP.

Then we investigate the transport property of the HISs in the two systems. Figure 7(a) gives the current–voltage (I–V) curves in the P configuration. For the tricene molecule, the current curve increases non-linearly in the two systems, where the maximum current achieves about 4.5 μA at 2.0 V. It is noticed that there is no threshold voltage in the I–V curve, which is induced by the presence of the spin-down HIS at the Fermi energy at zero bias (see Fig. 2(a)). The current increases more rapidly after 1.5 V, since the molecular orbitals start to contribute to the current at a large bias according to Fig. 5(a). For the octane molecule, the current is quite small, which is about three orders of magnitude less than that of the tricene molecule. This is because although the HISs appear near the Fermi energy, the component lacks π orbitals and has no obvious effect on the current.

Figure 7(b) shows the curves of SP *versus* voltage of the current under the bias voltage. Here the SP is defined as $\mathrm{SP}(V) = \left[I_\uparrow(V) - I_\downarrow(V)\right] / \left[I_\uparrow(V) + I_\downarrow(V)\right]$. We find that the current is spin-down-polarized for the tricene molecule. With the increasing bias voltage, the value of the SP decreases from -86% at 0.2 V to -20% at 1.0 V and then fluctuates. The trend of the change at low bias is similar to the scenario of the SP at Fermi energy shown in Fig. 6, while at large bias they differ since the current is contributed by all the HISs in the bias window. For the octane molecular junction, a rever-

sal of the SP is observed at several bias voltages. The maximum magnitude is less than −30% in the region of calculated bias voltage. The above results indicate that the HISs in the π-conjugated molecular junction work more efficiently on the current SP than those in the molecular junction without π orbitals. Furthermore, the SP of the current does not match the SP of PDOS at Fermi energy exactly, where the bias-induced evolution of the PDOS and the contribution from multi states in the bias window should be concerned.

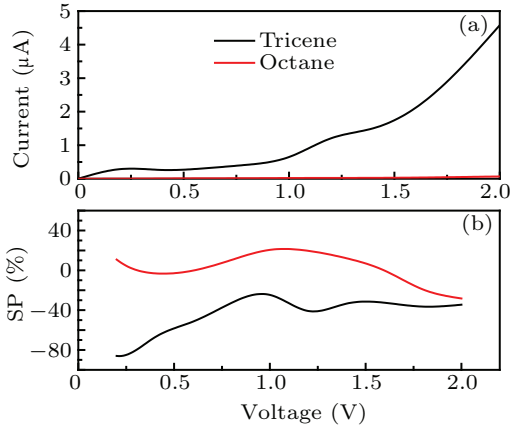


Fig. 7. (a) Current–voltage curves and (b) SP–voltage curves in P configuration.

Finally, the bias-dependent tunneling magnetoresistances (TMRs) of the two molecular junctions are compared with each other. The result is shown in Fig. 8, where the TMR is defined as $\mathrm{TMR}(V) = [I_{\mathrm{P}}(V) - I_{\mathrm{AP}}(V)]/I_{\mathrm{AP}}$ where $I_{\mathrm{P(AP)}}(V)$ is the current in the P (AP) configuration. For the octane molecular junction where the transport through the HIS is strongly inhibited, only a small TMR less than 8% is obtained in the region of calculated bias voltage, which is just slightly disturbed by the bias. However, for the tricene molecular junction, a much larger TMR as large as −54% is achieved. The TMR is sensitive to the bias voltage, which first decreases with bias from 44% at 0.2 V, and changes the sign after 0.4 V. The maximum TMR achieves −54% at 0.9 V, and then decreases again, where TMR stays at about 6% when the bias becomes large. These results show that the bias-induced modulation of the PDOS may change the sign of the TMR and enhance the spin valve functionality. By investigating the spin-dependent transmission spectrum at 0.2 V and 1.0 V, the mechanism of the TMR is further discussed. The results are shown in Fig. 9. Here only the result of the tricene molecular junction is given. At 0.2 V, an obvious spin-down transmission peak from the HIS contributes to the current in P configuration, while the corresponding peak in AP configuration is much smaller. This leads to a positive TMR. At 1.0 V, the spin-down HIS peak enters into the bias window completely. But the height in AP configuration turns higher than that in P configuration, therefore, causing a negative TMR effect. When the bias voltage is increased to 1.6 V, it is noticed that the transmission from the HIS turns very small, while the high LUMO transmission peaks enter into the bias window. Owing to the near spin degeneracy of the LUMO, the TMR as well as the SP of current is much weakened.

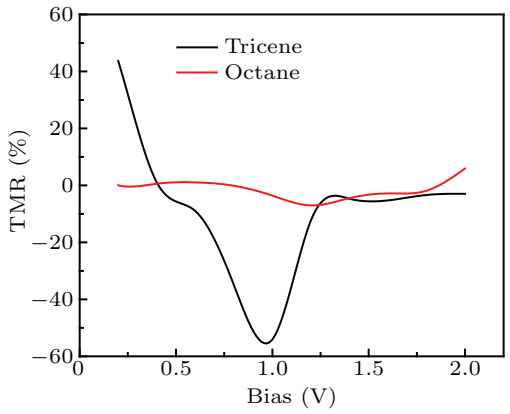


Fig. 8. Bias-dependent tunneling magnetoresistance in different molecular junctions.

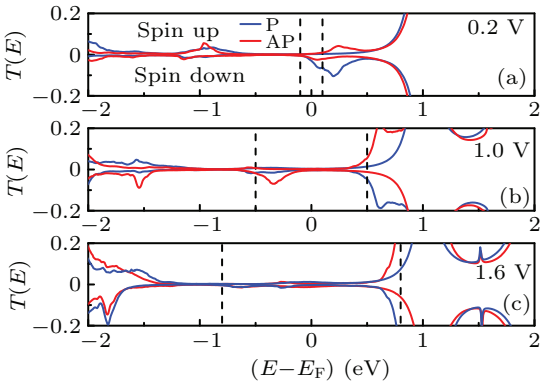


Fig. 9. Bias-dependent transmission spectrum of the Ni/tricene/Ni junction at (a) 0.2 V, (b) 1.0 V, and (c) 1.6 V in P (blue line) and AP (red line) configurations. The dashed lines indicate the bias window.

It should be mentioned that although the bias-induced reconstruction of the HIS is discussed mainly in P configuration, the situation in AP configuration is also investigated, and the results are not shown here due to the similarity in physics. At zero bias voltage, the HISs in AP configuration are spin degenerate. It is because the interfacial hybridization at the left interface and at right interface are antisymmetric due to opposite magnetizations of the electrodes. Applying a bias voltage, a similar splitting and shift of the HIS is also observed. The reconstruction of the HISs will break the spin degeneracy and give rise to diverse SP values around the Fermi energy.

Finally, it is noticed that the SP of the HIS also rely on the interface structure, *e.g.*, interfacial contact structure and anchoring groups.[24,40,41] Different interface structures generate different initial HISs at zero bias voltage. Applying a bias voltage, the bias-induced shift and reconstruction may lead to diverse SP values of the HISs around Fermi energy, which is expected to trigger off interesting effects on the transport property. A quantitative investigation deserves to be performed in the future.

4. Conclusions

In summary, we have investigated the evolution of the HIS with bias voltage and its transport properties in molecular junctions. Here we compare the tricene molecules with octane molecules, which are adsorbed to two Ni (111) electrodes via S anchoring group. The bias-induced splitting and shift of the HIS are observed in both molecular junctions. The reconstruction of the HIS under bias makes the SP value around the Fermi energy adjustable. A resulting sign inversion or enhancement of SP can be achieved by bias. The transport property calculation demonstrates that although the evolutions of the HISs are similar in the two junctions, their contributions to the spin-dependent transport are different. In the π-conjugated tricene molecular junction, the HISs provide efficient transmission, which leads to a relatively large current, SP of the current and TMR. Therein a bias-induced decrease of current SP and an inversion of TMR are further observed. In the octane molecular junction, the transport via the HIS is strongly inhibited accompanied with a small current, SP of current and TMR, which are not sensitive to the bias. This work indicates that the bias effect should not be ignored in the design of molecular spintronic devices with the utilization of molecular spinterface. Such a bias effect is expected to be more distinct in HIS based molecular devices rather than most of other molecular devices, which is due to the nature of localized states of the HISs.

Acknowledgements

Project supported by the National Natural Science Foundation of China (Grant Nos. 11974215, 21933002, and 11874242) and the Shandong Provincial Natural Science Foundation, China (Grant No. ZR2019MA043).

References

[1] Xiong Z H, Wu D, Vardeny Z V and Shi J 2004 *Nature* **427** 821
[2] Sun M F, Wang X C and Mi W B 2018 *J Phys Chem. C* **122** 3115
[3] Li Y Q, Kan H J, Miao Y Y, Yang L, Qiu S, Zhang G P, Ren J F, Wang C K and Hu G C 2020 *Chin. Phys. B* **29** 017303
[4] Li Y Q, Kan H J, Miao Y Y, Qiu S, Zhang G P, Wang C K and Hu G C 2020 *Physica E* **124** 114327
[5] Miao Y Y, Qiu S, Zhang G P, Wang C K, Ren J F and Hu G C 2021 *Physica E* **131** 114729
[6] Naber W, Faez S and Wiel W 2007 *J. Phys. D: Appl. Phys.* **40** R205
[7] Yakhmi J V and Bambole V 2012 *Solid State Phenomena* **189** 95
[8] Qi J S, Miao Y Y, Cui Y J, Qiu S, Zhao J M, Zhang G P, Ren J F, Wang C K and Hu G C 2021 *Results Phys.* **27** 104510
[9] Zeng J, Chen K Q and Zhou Y 2020 *Chin. Phys. B* **29** 088503
[10] Gu X R, Guo L D and Sun X N 2018 *Chin. Phys. B* **27** 107202
[11] Fert A 2008 *Rev. Mod. Phys.* **80** 1517
[12] Tyagi P and Friebe E 2018 *J. Magn. Magn. Mater.* **453** 186
[13] Sun D L, Yin L F, Sun C J, Guo H W, Gai Z, Zhang X G, Ward T Z, Cheng Z H and Shen J 2010 *Phys. Rev. Lett.* **104** 236602
[14] Sanvito S and Rocha A R 2006 *J. Comput. Theor. Nanosci.* **3** 624
[15] Gruber M, Ibrahim F, Boukari S, Joly L, Costa V D, Studniarek M, Peter M, Isshiki H, Jabbar H, Davesne V, Arabski J, Otero E, Choueikani F, Chen K, Ohresser P, Wulfhekel W, Scheurer F, Beaurepaire E, Alouani M, Weber W and Bowen M 2015 *Nano. Lett.* **15** 7921
[16] Methfessel T, Steil S, Baadji N, Großmann, N, Koffler K, Sanvito S, Aeschlimann M, Cinchetti M and Elmers HJ 2011 *Phys. Rev. B* **84** 224403
[17] Shi S W, Sun Z Y, Bedoya-Pinto A, Graziosi P, Li X, Liu X J, Hueso L, Dediu V A, Luo Y and Fahlman M 2014 *Adv. Funct. Mater.* **24** 4812
[18] Sanvito S 2010 *Nat. Phys.* **6** 562
[19] Cinchetti M, Dediu V A and Hueso L E 2017 *Nat. Mater.* **16** 507
[20] Atodiresei N, Brede J, Lazić P, Caciuc V, Hoffmann G, Wiesendanger R and Blügel S 2010 *Phys. Rev. Lett.* **105** 066601
[21] Djeghloul F, Gruber M, Urbain E, Xenioti D, Joly L, Boukari S, Arabski J, Bulou H, Scheurer F, Bertran F, Fèvre PL, Taleb-Ibrahimi A, Wulfhekel W, Garreau G, Hajjar-Garreau S, Wetzel P, Alouani M, Beaurepaire E, Bowen M and Weber W 2016 *J. Phys. Chem. Lett.* **7** 2310
[22] Atodiresei N, Caciuc V, Lazié P and Blügel S 2011 *Phys. Rev. B* **84** 172402
[23] Qiu S, Miao Y Y, Zhang G P, Ren J F, Wang C K and Hu G C 2019 *J. Magn. Magn. Mater.* **489** 165465
[24] Qiu S, Miao Y Y, Zhang G P, Ren J F, Wang C K and Hu G C 2019 *J. Magn. Magn. Mater.* **479** 247
[25] Gutiérrez R, Fagas G, Richter K, Grossmann F and Schmidt R 2003 *Europhys. Lett.* **62** 90
[26] Van Dyck C, Geskin V and Cornil J 2014 *Adv. Funct. Mater.* **24** 6154
[27] Barraud C, Seneor P, Mattana R, Fusil S, Bouzehouane K, Deranlot C, Graziosi P, Hueso L, Bergenti I, Dediu V, Petroff F and Fert A 2010 *Nat. Phys.* **6** 615
[28] Qiu S, Miao Y Y, Zhang G P, Ren J F, Wang C K and Hu G C 2020 *J. Phys. Chem. C* **124** 12144
[29] Okuyama H, Kitaguchi Y, Hattori T, Ueda Y, Ferrer NG, Hatta S and Aruga T 2016 *J. Chem. Phys.* **144** 244703
[30] Xie F, Fan Z Q, Chen K Q, Zhang X J and Long M Q 2017 *Org. Electron.* **50** 198
[31] Soler J M, Artacho E, Gale J D, García A, Junquera J, Ordejón P and Sánchez-Portal D 2002 *J. Phys: Condens. Matter.* **14** 2745
[32] Taylor J, Guo H and Wang J 2001 *Phys. Rev. B* **63** 245407
[33] Perdew J P, Burke K and Ernzerhof M 1996 *Phys. Rev. Lett.* **77** 3865
[34] Troullier N and Martins J L 1990 *Solid State Commun.* **74** 613
[35] Datta S 1995 *Electronic Transport in Mesoscopic Systems* (New York: Oxford University Press)
[36] Ferry D and Goodnick S M 1997 *Transport in Nanostructures* (Cambridge: Cambridge University Press)
[37] Yang J F, Zhou L, Han Q and Wang X F 2012 *J. Phys. Chem. C* **116** 19996
[38] Larade B, Taylor J, Zheng Q R, Mehrez H, Pomorski P and Guo H 2001 *Phys. Rev. B* **64** 195402
[39] Yu C J, Miao Y Y, Qiu S, Cui Y J, He G M, Zhang G P, Wang C K and Hu G C 2018 *J. Phys. D: Appl. Phys.* **51** 345302
[40] Zhang Z, Qiu S, Miao Y Y, Ren J F, Wang C K and Hu G C 2017 *Appl. Surf. Sci.* **409** 60
[41] Li Y, Zhang G P, Xie Z, Zhang Z, Ren J F, Wang C K and Hu G C 2016 *Chin. J. Chem. Phys.* **29** 344